Estuarine, Coastal and Shelf Science 172 (2016) 1–12

Contents lists available at ScienceDirect

Estuarine, Coastal and Shelf Science

journal homepage: www.elsevier.com/locate/ecss

Hyperspectral remote sensing of wild oyster reefs

Anthony Le Bris [a, b, *], Philippe Rosa [b], Astrid Lerouxel [b], Bruno Cognie [b], Pierre Gernez [b], Patrick Launeau [c], Marc Robin [a], Laurent Barillé [b]

[a] Université de Nantes, Institut Universitaire Mer et Littoral (FR_C 3473), LETG-Géolittomer (UMR 6554, CNRS), Campus Tertre, BP 81227, 44312, Nantes Cedex 3, France
[b] Université de Nantes, Institut Universitaire Mer et Littoral (FR_C 3473), Mer Molécules Santé (EA 2160), Faculté des Sciences et des Techniques, BP 92208, 44322, Nantes Cedex 3, France
[c] Université de Nantes, Institut Universitaire Mer et Littoral (FR_C 3473), Laboratoire de Planétologie et Géodynamique (UMR 6112, CNRS), Faculté des Sciences et des Techniques, BP 92208, 44322, Nantes Cedex 3, France

ARTICLE INFO

Article history:
Received 10 July 2015
Received in revised form
17 December 2015
Accepted 23 January 2016
Available online 28 January 2016

Keywords:
Benthos
Crassostrea gigas
Hyperspectral
Oyster reefs
Remote sensing
Tidal flats

ABSTRACT

The invasion of the wild oyster *Crassostrea gigas* along the western European Atlantic coast has generated changes in the structure and functioning of intertidal ecosystems. Considered as an invasive species and a trophic competitor of the cultivated conspecific oyster, it is now seen as a resource by oyster farmers following recurrent mass summer mortalities of oyster spat since 2008. Spatial distribution maps of wild oyster reefs are required by local authorities to help define management strategies. In this work, visible-near infrared (VNIR) hyperspectral and multispectral remote sensing was investigated to map two contrasted intertidal reef structures: clusters of vertical oysters building three-dimensional dense reefs in muddy areas and oysters growing horizontally creating large flat reefs in rocky areas. A spectral library, collected *in situ* for various conditions with an ASD spectroradiometer, was used to run Spectral Angle Mapper classifications on airborne data obtained with an HySpex sensor (160 spectral bands) and SPOT satellite HRG multispectral data (3 spectral bands). With HySpex spectral/spatial resolution, horizontal oysters in the rocky area were correctly classified but the detection was less efficient for vertical oysters in muddy areas. Poor results were obtained with the multispectral image and from spatially or spectrally degraded HySpex data, it was clear that the spectral resolution was more important than the spatial resolution. In fact, there was a systematic mud deposition on shells of vertical oyster reefs explaining the misclassification of 30% of pixels recognized as mud or microphytobenthos. Spatial distribution maps of oyster reefs were coupled with *in situ* biomass measurements to illustrate the interest of a remote sensing product to provide stock estimations of wild oyster reefs to be exploited by oyster producers. This work highlights the interest of developing remote sensing techniques for aquaculture applications in coastal areas.

1. Introduction

Pacific oyster (*Crassostrea gigas*) is the main bivalve species cultivated worldwide (FAO, 2006; Forrest et al., 2009). This species was introduced into European waters in the seventies to replace the Portuguese oyster (*Crassostrea angulata*) which had been greatly reduced by a large-scale epizootia outbreak (Grizel and Héral, 1991). With the increase of water temperature, spawning and larval survival were gradually observed toward northern latitudes, and oysters progressively colonized intertidal areas, forming dense reefs (Diederich, 2005; Dutertre et al., 2010). Feral *C. gigas* is now considered as an invasive species with different impacts on receiving communities (Troost, 2010). Among these impacts, the most obvious is a direct spatial and trophic competition with local species such as the blue mussel (*Mytilus edulis*) (Diederich, 2005, 2006; Schmidt et al., 2008; Troost, 2010; Markert et al., 2013; Green et al., 2013). Wild oysters also became trophic competitors with cultivated conspecifics causing slower growth and economic losses for the oyster farmers (Cognie et al., 2006). In France, they were considered as a pest by the oyster industry. However since 2008, recurrent mass summer mortalities of oyster spat were

* Corresponding author. Université de Nantes, Institut Universitaire Mer et Littoral (FR_C 3473), LETG-Géolittomer (UMR 6554, CNRS), Campus Tertre, BP 81227, 44312, Nantes Cedex 3, France.
E-mail address: anthony.le-bris@univ-nantes.fr (A. Le Bris).

http://dx.doi.org/10.1016/j.ecss.2016.01.039
0272-7714/

observed along the European coasts with a subsequent decline of the cultivated stock (Cotter et al., 2010; Pernet et al., 2012; Girard and Pérez Agúndez, 2014). As a consequence, the status of the wild oyster changed radically and in some areas oyster producers envisaged exploiting their population as a resource to compensate for their losses. This situation induced conflicts with recreational and professional fishermen generating a need to map and manage wild oyster reefs. However, in many areas of the west European Atlantic coast, these reefs grow in rocky areas within large intertidal mudflats notoriously inaccessible and hard to sample. Traditional ground surveys are therefore time-consuming, expensive and require a substantial human effort in these areas (Cognie et al., 2006). Thus, there is a growing interest and need for the development of reliable remote sensing tools to provide a synoptic view of wild oyster reefs in coastal areas.

Aerial photography has been used to detect live and dead oyster reefs using brightness differences (Grizzle et al., 2002; Kater and Baars, 2004). However, the specific spectral properties related to reflected electromagnetic radiations at different wavelengths cannot be exploited with panchromatic photographs. A preliminary investigation with a multispectral resolution was tested for oyster mapping in South Carolina (NOAA, 2003). More recently, microwave remote sensing with synthetic aperture radar (SAR) was used to map bivalve beds (mussels and oysters) in intertidal areas (Choe et al., 2012; Gade et al., 2014; Nieuwhof et al., 2015). Choe et al. (2012) showed that polarimetric characteristics of SAR images can be used to distinguish surface roughness of oyster reefs from that surrounding mudflat. However, this technique did not permit the discrimination of bivalve species (Gade et al., 2014; Nieuwhof et al., 2015), and was not tested to discriminate distinct tridimensional configuration (e.g. horizontally vs. vertically developed oysters) as can be observed for oyster reefs. Additional optical data in visible and near-infrared domains could improve classifications of intertidal mudflats (Van der Wal and Herman, 2007) and oyster reefs detection (Dehouck et al., 2011). Visible-near infrared (VNIR) data are very useful to map intertidal vegetation such as seagrass (Pasqualini et al., 2005; Barillé et al., 2010) or microphytobenthic biofilms (Brito et al., 2013; Benyoucef et al., 2014) but the richness of absorption bands due to photosynthetic and accessory pigments cannot *a priori* be exploited for bivalve beds. Moreover, the broadband resolution of many multispectral VNIR sensors may be a limit for their detection (Girouard et al., 2004). This restriction could be overcome by using high resolution hyperspectral data. Surprisingly, this technique has only been tested by Schill et al. (2006) to map eastern oyster reefs (*Crassostrea virginica*) based on their spectral reflectance. They suggested that hyperspectral remote sensing could be useful for mapping shellfish resources but observed a high spectral variability within the oyster habitat. Therefore, evaluating the efficiency of hyperspectral data remains to be assessed and generalized to different ecosystems, species and reef typology. For instance, none of the studies previously cited using radar data considered the common situation in western Atlantic bays where oyster reefs can be found in intertidal flats but also in adjacent rocky areas growing with a distinct configuration.

This study aimed to produce spatial distribution maps of wild oyster reefs for two contrasted reef typologies found in mudflats and rocky areas using hyperspectral data from the airborne sensor HySpex. A comparison was performed between HySpex data and SPOT satellite HRG multispectral data to evaluate the role of the sensor's spectral resolution. HySpex maps were spatially and spectrally degraded to compare overall accuracy at different resolutions. In this study, spectral signatures of oyster shells have been analyzed using *in situ* spectroradiometric measurements obtained for different conditions. Finally, we propose a simple method using reef distribution maps and *in situ* measurements of oyster biomass to illustrate the interest of a remote sensing product for the management of this resource at the scale of a shellfish ecosystem.

2. Materials and methods

2.1. Study area

Bourgneuf Bay, located south of the Loire estuary on the French Atlantic coast (47°02′ N, 2°07′ W) (Fig. 1), is a macrotidal bay with a maximum tidal amplitude of 6 m. 100 km^2 of the total bay area (340 km^2) is intertidal. It is a site of extensive aquaculture of the oyster *C. gigas* (Thunberg), ranking fifth in France with a production of 7000 metric tons on 1000 ha of on-bottom cultures. The intertidal zone comprises large mudflats and rocky areas but smaller rocky spots are found in the middle of the mudflat. Two types of wild oyster reefs can be observed: reefs situated in rocky spots within the mudflat which are hardly accessible (Fig. 1, Site 1) and those found in the large rocky areas with a much easier access (Fig. 1, Site 2).

2.2. Typology of wild oyster reefs

Two distinct forms of colonization can be observed: clusters of vertical oysters building three-dimensional dense reefs in the muddy area (Fig. 2A, B) and oysters growing horizontally creating large flat reef structures in rocky areas (Fig. 2D, E). The first form is very similar to the one described for South-Carolina's oyster reefs (NOAA, 2003). A further distinction can be made according to the mud deposition. In the muddy area, oyster shells were dark and partially covered by mud, while in rocky areas, in the absence of any mud deposition, oyster shells had a brighter color. Spectral responses of each reef were obtained with a field portable spectroradiometer ASD FieldSpec3®, measuring the radiance (mW cm^{-2} nm^{-2} sr^{-1}) between 350 and 2500 nm with a spectral sampling interval of 1.4 nm up to 1050 nm and 2 nm up to 2500 and a spectral resolution from 3 to 10 nm. Surface reflectance was determined by measuring the light reflected by a ~99% reflective Spectralon® reference panel (Fig. 2C, F).

2.3. Image pre-processing

Bourgneuf bay was imaged by a HySpex VNIR 1600 camera on September 21st, 2009, during an airborne campaign. This sensor provides a spectral resolution of 4.5 nm in 160 contiguous channels between 400 and 1000 nm. A mosaic of around 20 flight lines over the study area was obtained for a high spatial resolution of 1 m^2 per pixel. A multispectral image was also acquired by the HRG sensor of SPOT-5 satellite on September 8th, 2009. It is characterized by 4 wide bands (500–590; 610–680; 780–890; 1580–1750 nm) and a spatial resolution of 100 m^2 per pixel. Both hyperspectral and multispectral images were acquired at low tide, in cloud-free conditions (<10%). Images were calibrated to ground reflectance using the FLAASH (Fast Line-of-sight Atmospheric Analysis of Spectral Hypercubes) atmospheric corrections module, incorporating the MODTRAN4 transfer code (Matthew et al., 2000). For Bourgneuf Bay, a middle latitude summer atmospheric model was used combined with a maritime aerosol model. MNF (Minimum Noise Fraction) transformations combined with a band-pass filter of 9 nm were applied to the images to remove noise and redundant information. A geographical mask of the terrestrial part and a radiometric mask of the water were applied to identify the intertidal area. Within this area, another mask was applied to distinguish all rocky surfaces from the mudflat itself since wild oysters do not develop directly in the mud, and are systematically associated to a hard substrate. This mask was performed using an X-band SAR

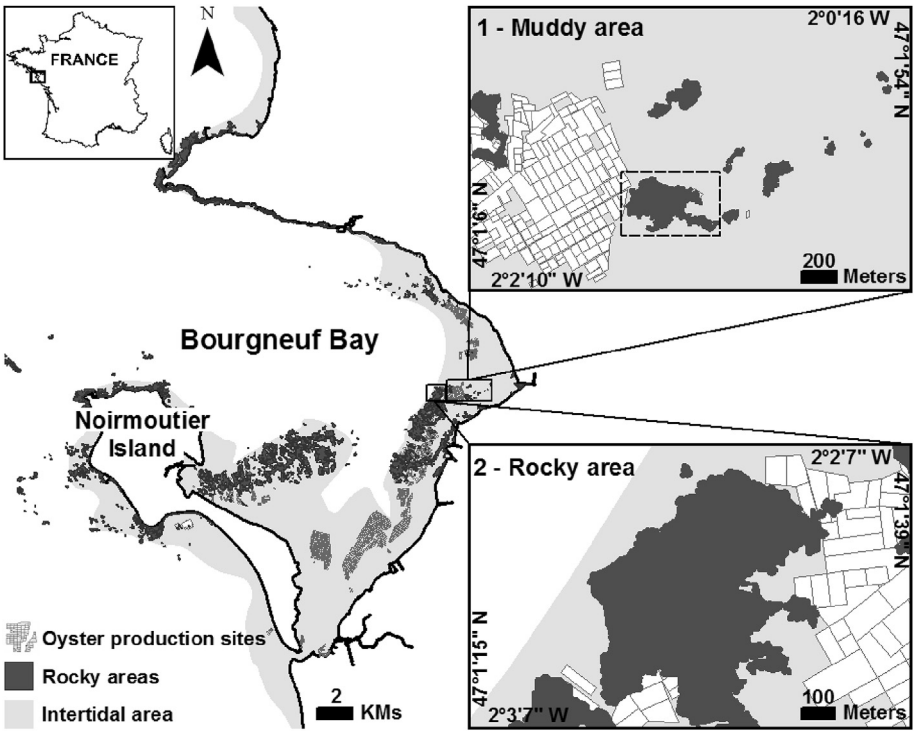

Fig. 1. Bourgneuf Bay study area with sample site locations. 1: Muddy rocks mainly colonized by clusters of vertical oysters surrounded by mudflats (2°02′35″W, 47°01′30″N); the dash rectangle corresponds to the map Fig. 4. 2: Large rocky areas mainly colonized by horizontal oyster reefs and surrounded by sandy-muddy substrates (2°01′20″W; 47°01′21″N).

image (9.65 GHz) obtained from the TerraSAR-X sensor. These radar data were acquired at low tide in HH and HV polarization with an incident angle of 44.1° and a spatial resolution of 2.75 m. The sensitivity of the backscattering coefficient (σ°) to surface roughness allowed the differentiation of roughened rocky areas from smoother mudflat areas in the intertidal area (Fig. 5A and 6A). Only rocks delimited by the radar image were used for hyperspectral and multispectral classifications using HySpex and SPOT sensors.

2.4. Oyster mapping methodologies

2.4.1. Field spectroradiometry

Reflectance spectra of the main sediments and marine vegetation that can be present within a pixel were recorded in the field using the ASD FieldSpec3®. Spectral responses of microphytobenthos (benthic unicellular photoautotrophs typically composed of diatoms, dinoflagellates, euglenoids or cyanobacteria), bare mud, macroalgae, and other targets found in the intertidal area around or within oyster beds were measured in the VNIR range between 400 and 900 nm, as absorption by the water is strong beyond 900 nm. A spectral resampling was applied on the *in situ* spectral library to match the specific spectral range of the hyperspectral or multispectral images. Spectral signatures were measured along transects and averaged to calculate a mean spectrum for each surface. All spectroradiometer readings were taken under clear sky conditions close to dates of image acquisitions. *In situ* spectral signatures were also acquired in different seasons (March, June, July and November), for spring and neap tides and with acquisitions in a 2-h interval around the low tide to take into account variations due to desiccation. This work also benefited from a library of intertidal spectra collected during previous field campaigns (Combe et al., 2005; Barillé et al., 2010; Kazemipour et al., 2012).

2.4.2. Spectral Angle Mapper

The supervised Spectral Angle Mapper (SAM) classification (Kruse et al., 1993) was performed to identify wild oyster reefs, using a spectral library obtained *in situ* with spectroradiometric measurements (Fig. 3). This classifier was selected because it has been widely applied for intertidal and marine benthic environment (e.g. Belluco et al., 2006; Kutser and Jupp, 2006), and had been used successfully in the studied site to map microphytobenthos (Kruse, 2003; Combe et al., 2005). In addition, classically supervised classification methods, more sensitive to solar illumination were tried. For example minimum distance and maximum likelihood classifications or texture filters based on variance and entropy were tested but did not give satisfying results. In the SAM method the spectral angle is independent of the length of the two vectors, which has the interesting property of removing albedo variations and topographic effect (Kruse, 2003; Combe et al., 2005). Spectral the angle (θ) between spectra for each band considering them as n-dimensional vectors in space (where n equals the number of hyperspectral or multispectral bands):

$$\theta(\vec{t},\vec{r}) = \cos^{-1}\left(\vec{t}\cdot\vec{r}/\|\vec{t}\|\cdot\|\vec{r}\|\right) \quad (1)$$

Where *t* is the unknown spectrum from pixels of images and *r* the reference spectrum from the field library. Small deviation indicates strong similarity between the unknown spectrum and the reference. Pixels were assigned to a determined class according to a maximum threshold (in radians) above which they were not classified.

2.4.3. Validation

Accuracy assessments of SAM classifications were performed using a confusion matrix (Congalton, 1991). The Kappa coefficient (K) and the overall accuracy (OA) were chosen as measures of agreement between classification results and validation data

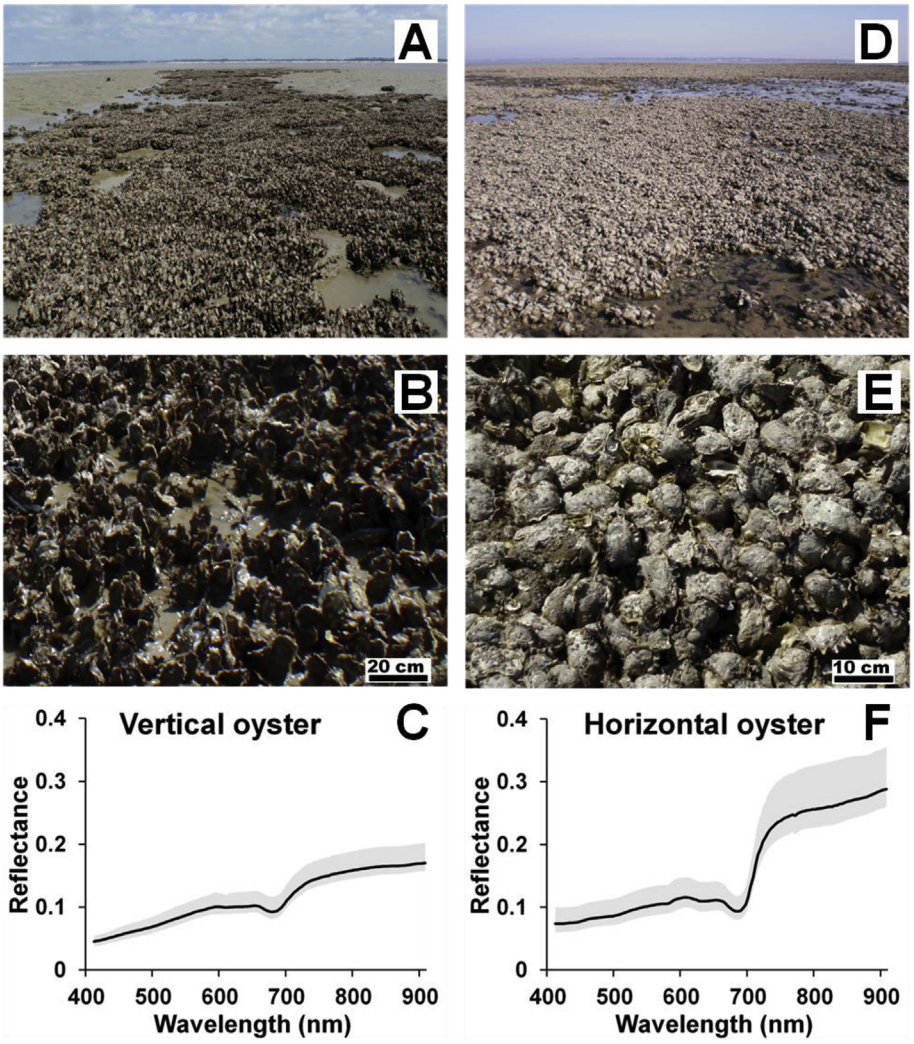

Fig. 2. Typology of wild oyster reefs; left: clusters of vertical oysters surrounded by mudflats (A), details of vertical oyster clusters (B) and their spectral signature (C) and right: horizontal colonization of large rocky areas (D), details of horizontally-growing oysters (E) and their spectral signature (F). Gray areas around the mean values are delimited by min and max spectrum.

(Belluco et al., 2006). The latter is based on the comparison with Regions Of Interest (ROIs) identified *in situ* with GPS for each class. Each ROI was randomly selected and covered areas several times larger than the coarser pixel size. Overall accuracy was computed by dividing the number of validation pixels correctly classified by the total number of validation pixels irrespective of the class, whereas the kappa coefficient takes into account all the classes as well as the pixels wrongly classified due to a random agreement:

$$K = (p_o - p_c)/(1 - p_c) \quad (2)$$

Where p_o represents the proportion of correctly classified validation sites and p_c, the proportion of agreement occurring by chance. The kappa interpretation is defined by means of ranks starting from 0 to 0.20 for a poor agreement up till 0.80–1 for an almost perfect agreement. These indices were applied for both reef types in muddy and rocky areas and for HySpex and SPOT-5 images. Spatial and/or spectral degradations of the hyperspectral image were performed: 1) to obtain a high spectral resolution (HySpex 160 bands) associated to a lower spatial resolution (100 m^2 of SPOT-5), and 2) a low spectral resolution of 3 large bands of SPOT-5 associated to a high spatial resolution (1 m^2 of HySpex) in order to analyze the effect of the spatial and spectral resolution on the classification results.

2.5. Estimation of wild oyster stock

Oyster biomass cannot be directly estimated by photointerpretation or remote sensing (undetectable multi-layers) and to assess wild oyster stock at the scale of an ecosystem, surface estimation must be combined with biomass field measurements. A previous estimation of wild oyster stocks had been performed in this study site using aerial orthophotographs associated to a systematic field sampling of oyster biomass using 0.25 m^2 quadrats (Cognie et al., 2006). Among the rocky areas, these authors did not discriminate oyster reefs and macroalgal belts, and the sampling strategy was applied to the total rocky surfaces. Field observations revealed that there are oysters under the macroalgal cover even though the density is much less important compared to oyster reefs. This previous method proposed by Cognie et al. (2006) based on sampling strategy applied to the entire rocky surface, was used as a reference to compare the approach proposed in this study (Fig. 4). For the estimation of rocky areas, we used TerraSAR-X sensor which is sensitive to surfaces roughness. A systematic sampling was applied to the total surfaces (rocky areas and rocks within the mudflats) with 180 sampling points. This was considered as the maximal sampling effort since for one point (one quadrat) it could

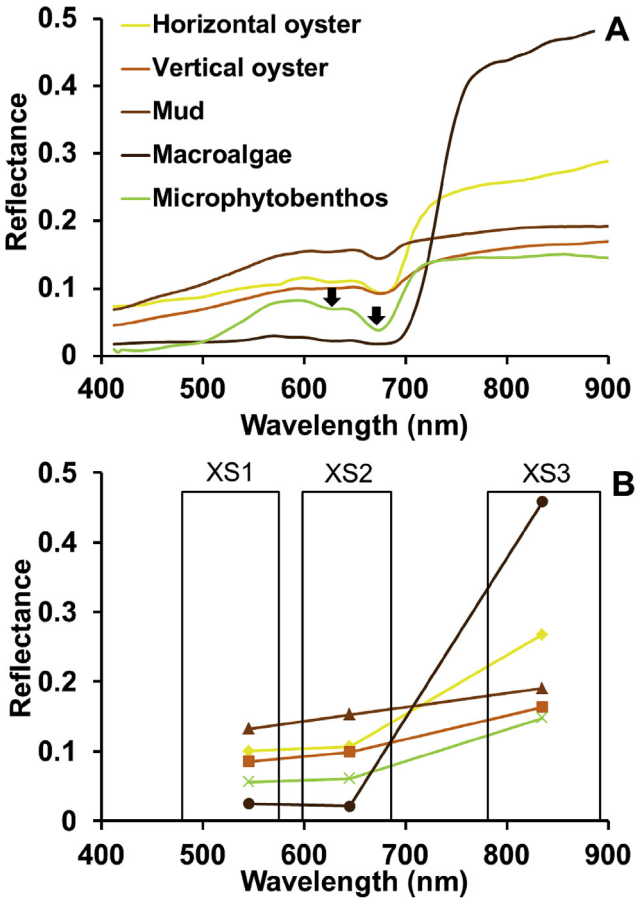

Fig. 3. Spectral signatures acquired by an ASD FieldSpec® spectroradiometer and used in the spectral library (For clarity not all spectra are shown). Spectral resampling to the HySpex resolution (A) and to the 3 spectral bands of SPOT-5 resolution (B). Black arrows represent spectral absorptions of the chlorophyll *c* at 632 nm and chlorophyll *a* at 673 nm. Histograms represent the position and spectral width of SPOT bands.

take up to half an hour to collect oysters tightly attached together and to the substratum. For each 0.25 m^2 quadrat, oyster biomass (total weight) was measured with an electronic balance, and expressed in $kg.m^{-2}$. The stock was defined by the product of the surface by the average oyster biomass per m^2. For the estimation based on HySpex data, 3 classes were used: horizontal oyster reefs, vertical oyster reefs, and macroalgal belts. To sample the oyster biomass a stratified random sampling was applied (Krebs, 1989), and it was decided to reduce the sampling effort by three, with 60 sampling points, equally distributed (n = 20 per class) since the three classes covered approximately the same surfaces.

2.6. Statistical analysis

All statistical analysis were conducted using XLSTAT 10 software (Addinsoft, France). The normality and heteroscedasticity of data distributions were tested before each analysis using the Shapiro test. Oyster biomass means were compared using the t-test. Mann–Whitney tests were used to compare stock assessments between a field systematic survey and a remote sensing estimation.

3. Results

3.1. Field spectral reflectance

The spectral shapes of the two types of oysters were generally similar in the visible range (between 400 and 700 nm) with a slightly steeper slope at blue-green wavelengths for vertical oysters (Fig. 2C, F). A striking common feature was an absorption band at 673 nm, characteristic of chlorophyll-*a*, and suggesting the permanent presence of photosynthetic organisms on the shells. This absorption band is the fingerprint of marine vegetation as shown in spectra of macroalgae and microphytobenthos (Fig. 3A). However, there were no macroalgal epibionts visible at the surface of oyster shells whatever their types (vertical. vs. horizontal). This suggests that the 673 nm absorption band was associated to unicellular organisms that were not detected visually. The spectrum of microphytobenthos, which develop biofilms on muddy sediments, systematically showed another absorption band at 632 nm (Fig. 3A). This absorption is due to chlorophyll *c* and identifies the class of diatoms. This absorption, although less pronounced, could be observed on the spectral response of horizontally developed oysters (Fig. 3A). These spectral features could only be detected with the hyperspectral resolution. After a spectral re-sampling at the spectral resolution of the 3 large SPOT-HRG bands (Fig. 3B), these pigment absorptions disappeared and spectral shapes tended to be similar in the visible part. In the Near-Infra Red (NIR, 700–900 nm), spectral reflectance was clearly higher for horizontal oysters than for those growing vertically (Fig. 2C, F). The flatter surface of horizontal oyster reefs probably explains these NIR differences. The vertical oyster reefs showed systematically a lower NIR plateau and this difference could still be detected at lower spectral resolution (Fig. 3B). In fact, vertical oysters often had a spectral shape that resembles that of mud (Fig. 3A), which tends to cover this type of reef.

3.2. Oyster identification

Two examples of maps obtained with the SAM classifications are presented respectively a rocky zone within the muddy area where oysters grow mainly vertically (Fig. 5) and a portion of the large rocky area where oyster grow mainly horizontally (Fig. 6). With the hyperspectral resolution, it was possible to detect oysters on the rocky zone within the muddy area as well as macroalgae and microphytobenthos (Fig. 5C). The latter could even be observed on the orthophotograph as brown-green biofilms covering most of the mudflat (Fig. 5B). Consistent spatial variations of microphytobenthos were identified (Fig. 5C), with higher biomass detected in the vicinity of a channel next to the cultivated oyster areas (see Combe et al., 2005). Biofilms of low biomass of microalgae were also detected within the rocky area delimited by SAR processing (Fig. 5C). This was confirmed *in situ*, and corresponds to muddy patches colonized by microphytobenthos, contributing to the fragmented aspect of the vertical-oyster reef (Fig. 2A). With the multispectral data, SAM did not correctly discriminate oyster classes from microphytobenthos and most of the mudflat was identified as oyster reefs (Fig. 5D). Macroalgae observable as dark spots on the orthophotograph (Fig. 5B) was the only class that showed a consistent distribution on the SPOT image (Fig. 5D).

For the rocky area, SAM maps obtained with HySpex images identified large areas of horizontal-oyster reefs bordered by smaller zones of vertical-oyster reefs in the lower intertidal area, in accordance with field observations (Fig. 6C). Similarly, it was possible to detect the many intertidal pools colonized by macroalgae, which characterize this rocky area. That was not the case for the multispectral image (Fig. 6D). Moreover, oyster reefs got confused with microphytobenthos, while macroalgae were the only class consistently identified with SPOT-5 image (Fig. 6D). In addition to this general description, *in situ* GPS acquisitions were used to quantitatively assess the accuracy of these SAM classifications.

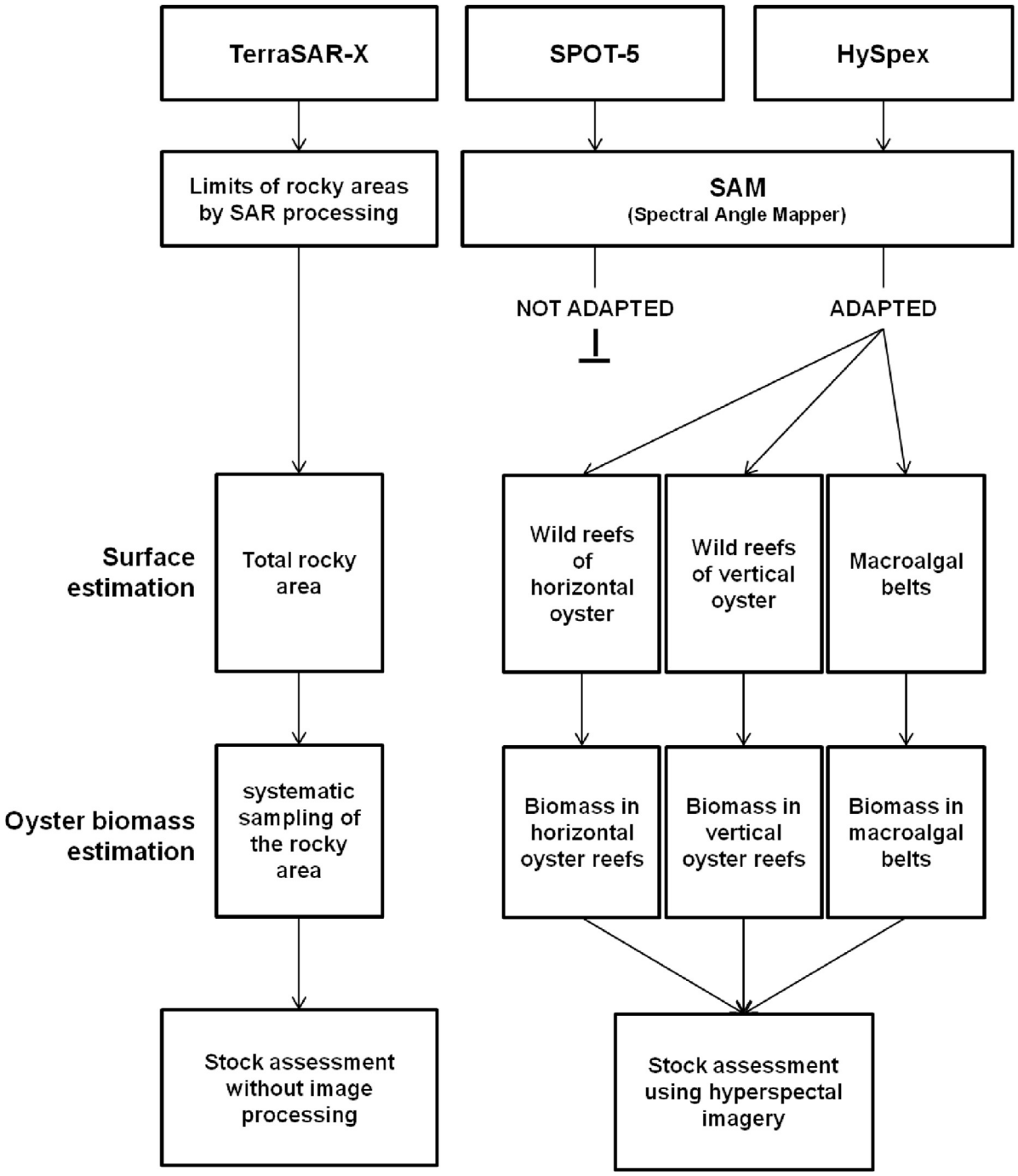

Fig. 4. Methodologies for estimating wild oyster stocks based on surface estimations (systematic sampling applied to the total rocky areas delimited by SAR processing vs. stratified sampling applied to classes identified by hyperspectral processing) coupled to field biomass measurements.

3.3. SAM classification accuracy

The overall accuracy and kappa coefficient calculated from the confusion matrices confirmed that the best results were obtained using the HySpex image whatever the type of oyster reef (muddy area with vertical oysters vs. rocky area with horizontal oysters) (Table 1). The lower spectral (3 bands) and spatial (100 m^2) resolutions of SPOT-5 resulted in a significant decrease of accuracy, with kappa coefficients between 0.23 and 0.31 compared to 0.59 and 0.68 for HySpex. When comparing the spatially or spectrally degraded HySpex images, it was clear that the spectral resolution was greater than the spatial resolution, to correctly identify the classes (Table 1). For HySpex spectrally degraded to SPOT bands, the kappa coefficient dropped to 0.30 in the muddy area, close to the value obtained with the multispectral image. Brown macroalgae were the best classified throughout the different resolutions, confirming that this type of vegetation could be identified whatever the available number of bands. The full confusion matrix for HySpex (Table 2) revealed that horizontal oysters in the rocky area were correctly classified at 78.1% while 14.7% were assigned to the vertical-oyster class, such that oyster reefs was generally identified at approx. 92.8%. However, vertical oysters in the muddy area were classified at 69.3% while the

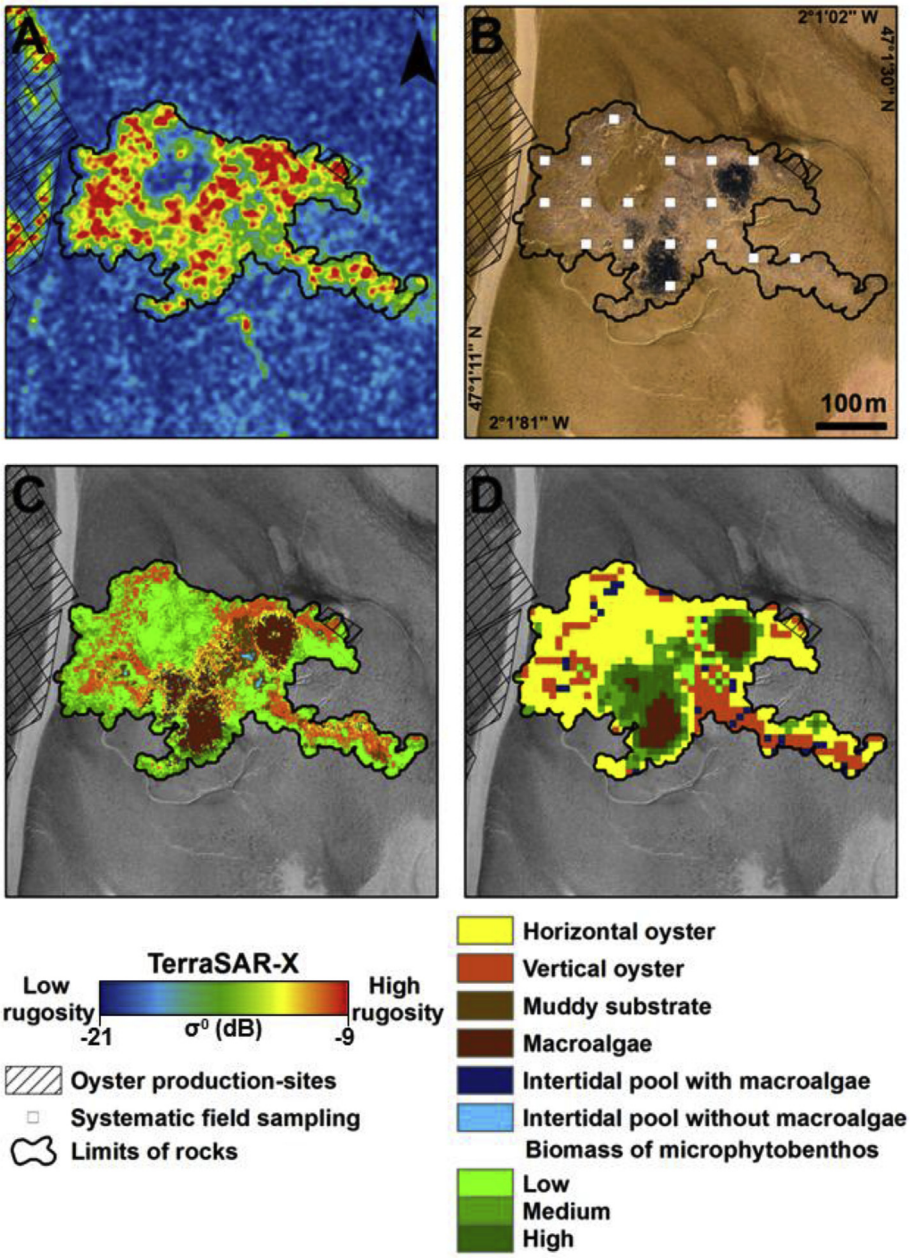

Fig. 5. SAM classification based on a field spectral library and applied to muddy rocks mostly colonized by vertical oysters (Fig. 1 site 1 – dash rectangle). (A) Surface scattering of the HH polarization on TerraSAR-X image. (B) The field sampling effort for biomass measurements is represented on an aerial photograph in true color. Comparison between hyperspectral data (C) and multispectral data (D) acquired by HySpex and HRG SPOT5 sensors respectively.

remaining pixels were misclassified as microphytobenthos (12.1%) or mud (14.1%). Indeed, rocky patches in the muddy area are characterized by frequent sub-pixel mixtures of oysters, mud and microphytobenthos which were more difficult to discriminate despite the high spatial and spectral resolutions of HySpex data.

3.4. Field biomass and stock assessments

The biomass of vertically growing oysters in muddy areas reached an average of 42 $kg.m^{-2}$, which is significantly higher than the mean biomass of 16 $kg.m^{-2}$ for horizontal oysters growing in rocky areas (Fig. 7; t-test, $p < 0.05$). The average oyster biomass found in macroalgal belts showed no significant difference (t-test, $p > 0.05$) between muddy and rocky areas with 2.8 $kg.m^{-2}$ and 1.8 $kg.m^{-2}$ respectively. However, these oyster biomasses in areas colonized by dense macroalgae were significantly lower (t-test, $p < 0.05$) than those measured in oyster reefs regardless of the vertical or horizontal configuration. These different biomasses were subsequently used to compare oyster stock estimations in two test areas (rocky vs. muddy) shown in Figs. 5 and 6, and using surfaces based either on the total rocky areas or oyster classes identified by hyperspectral images (Fig. 8). A stratified random sampling was applied using HySpex surface estimations and compared to a reference based on a systematic survey applied indistinctly to a total surface area delimited by SAR images (e.g. Figs. 5B and 6B). In the rocky area, there were no significant differences between the two stock estimations, in spite of a sampling three times smaller effort to estimate the biomass in the surfaces identified by HySpex

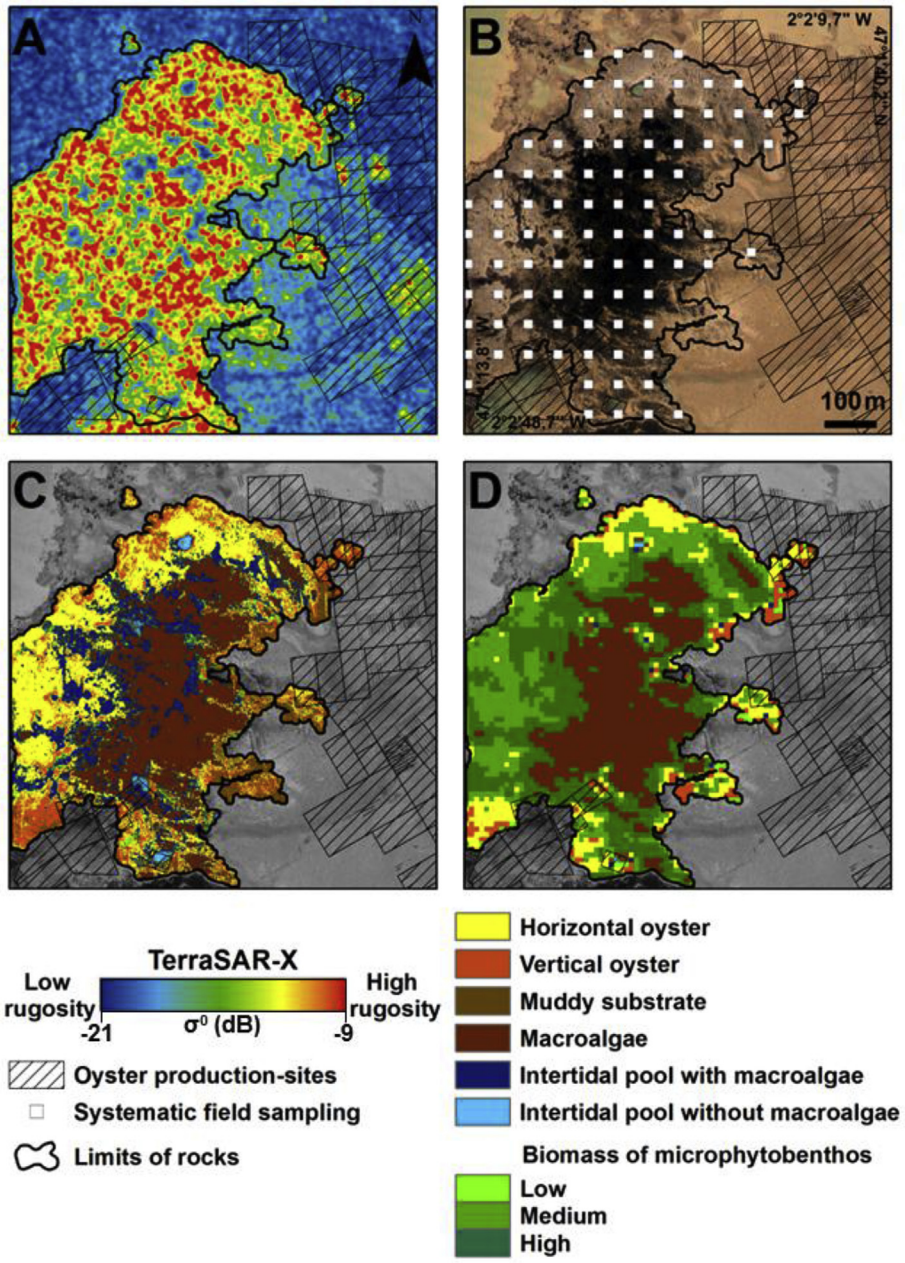

Fig. 6. SAM classification based on a field spectral library and applied to a large rocky area mostly colonized by horizontal oysters (Fig. 1 site 2). (A) Surface scattering of the HH polarization on TerraSAR-X image. (B) The field sampling effort for biomass measurements is represented on an aerial photograph in true color. Comparison between hyperspectral data (C) and multispectral data (D) acquired by HySpex and HRG SPOT5 sensors respectively.

(vertical oyster reef, horizontal oyster reef, macroalgal belts) (Fig. 8. Mann–Whitney, $p > 0.05$). However, in the muddy test area, the wild oyster stock estimated with hyperspectral data was significantly lower than the one based on the traditional survey used as a reference (Fig. 8. Mann–Whitney, $p < 0.05$).

4. Discussion

The analysis of SAM classifications obtained from hyperspectral processing revealed that it was possible to distinguish wild intertidal oyster reefs, using an *in situ* spectral library, but variable accuracy was obtained depending on the reef typology. Schill et al. (2006) have done pioneering work showing the interest of VNIR hyperspectral remote sensing for mapping intertidal shellfish resources in the southeast US. However, the typology of wild reefs formed by the American oyster *C. virginica* in Florida or Louisiana is more diverse than those described in our study (Grizzle et al., 2002). Indeed, Schill et al. (2006) observed a high degree of spectral variability within the oyster habitat particularly with vertical standing oysters and suggested that the interest of using an *in situ* spectral library was marginal. The automated techniques they used to extract endmembers from images have been successfully applied in several studies (Tompkins et al., 1997; Elmore et al., 2000; Quental et al., 2013), and this technique is particularly useful when it is difficult to obtain ground truth data (Purkis and Pasterkamp, 2004; Rosso et al., 2005). In our case, the use of a classification method based on an *in situ* spectral library gave better results than automatic endmember extraction methods, and it can be applied retrospectively on multi-

Table 1
Overall accuracy of the SAM classification for hyperspectral and multispectral data. HySpex data was also degraded at SPOT spectral or spatial resolution. Values indicate the percentage of correctly classified pixels relative to ground truth GPS data for each class. The kappa coefficient calculated with both correctly and wrongly classified pixels relative to each class.

	SAM classes	HySpex	SPOT	HySpex (Spatial degradation)	HySpex (Spectral degradation)
Muddy area (Site 1)	Horizontal oyster	40.2	23.6	30.5	24.6
	Vertical oyster	69.3	40.0	63.3	32.1
	Macroalgae	91.7	95.3	90.2	88.4
	Microphytobenthos	91.1	22.6	80.4	14.0
	Muddy substrate	53.2	0.3	44.0	52.2
	Overall accuracy	71.7	47.5	65.9	44.3
	Kappa coefficient	0.59	0.31	0.51	0.3
Rocky area (Site 2)	Horizontal oyster	78.1	8.6	58.5	63.8
	Vertical oyster	62.1	32.5	60.7	31.7
	Macroalgae	97.5	92.6	98.3	95.6
	Intertidal pool with macroalgae	63.8	0.4	54.7	18.1
	Muddy substrate	49.5	28.0	49.5	49.1
	Overall accuracy	75.5	32.6	67.4	54.8
	Kappa coefficient	0.68	0.23	0.58	0.45

Table 2
Complete confusion matrix for hyperspectral data for both horizontal and vertical reefs classes. Values indicate the percentage of correctly classified pixels. Lines correspond to classes of the SAM classification while columns correspond to the ground truth GPS acquisition.

		Vertical oyster
Muddy area (Site 1)	Horizontal oyster	3.4
	Vertical oyster	69.3
	Macroalgae	0.1
	Microphytobenthos	12.1
	Mud	14.1
	Intertidal pool with macroalgae	0.1
	Intertidal pool without macroalgae	0.6
		Horizontal oyster
Rocky area (Site 2)	Horizontal oyster	78.1
	Vertical oyster	14.7
	Macroalgae	1.0
	Microphytobenthos	0.7
	Mud	1.3
	Intertidal pool with macroalgae	4.3
	Intertidal pool without macroalgae	0

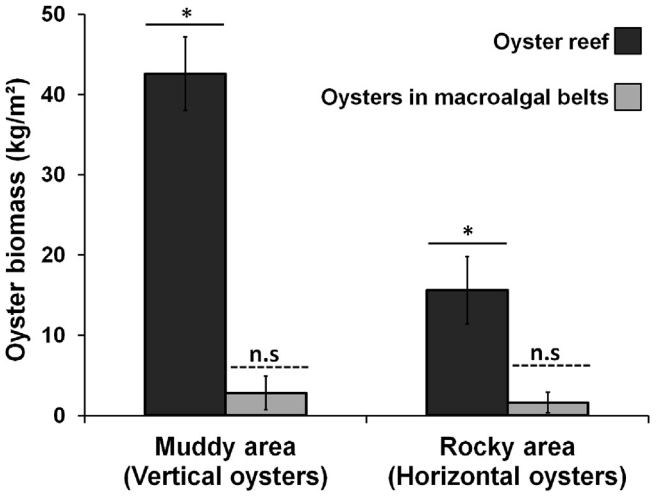

Fig. 7. Mean biomass of wild oysters *Crassostrea gigas* for both horizontal and vertical reefs. Black histograms represent the oyster biomass within oyster reefs without macroalgae while gray histograms present the oyster biomass under the macroalgal canopy (*Ascophyllum nodosum*, *Fucus vesiculosus*). Bars represent confidence intervals at 95%. Significant statistical analyses ($p < 0.05$) are indicated by *.

temporal images characterized by different spectral or spatial resolutions (Purkis and Pasterkamp, 2004; Leiper et al., 2014). This represents a minor technical divergence between our two studies, and the hyperspectral data clearly offer possibilities for more accurate large-scale mapping of oyster reefs compared to traditional methods based on photointerpretation.

4.1. SAM classification accuracy

In this study, the accuracy of the method differed according to the reef type. It was lower for vertical reefs in the muddy area for which the overall accuracy (OA) was 71% due to a misclassification concerning mud and microphytobenthos. Oyster shells are characterized by intimate mixtures that are between the spectral responses related to the shell mineralogy (Aragonite), to the presence of mud and a microalgal biofilm, and very often to several epibionts such as cirripeds. Moreover, vertical oysters are characterized by a stronger heterogeneity at the pixel scale, with clusters of oysters and mud patches. Sub-pixel mixing is a recurrent constraint for class separation (Mumby and Edwards, 2002; Yamano and Tamura, 2004; Mishra et al., 2006) which can be overcome with linear unmixing models (Byrd et al., 2014), but the latter are not adapted for the non-linear processes inherent to intimate mixtures. Non-linear spectral mixture analysis may be used in such situations but they are more complex and the results can be difficult to interpret (Chen and Vierling, 2006). To map vertical oyster reefs with a higher accuracy will be a challenge in muddy areas for VNIR sensors. The OA was higher in the rocky area with 78% of pixels correctly classified as horizontal oysters and 93% of pixels correctly classified as oyster reef. Interestingly, the two main types of intertidal vegetation, macroalgae and microphytobenthos, were consistently well classified (from 91 to 97%) which is a real advantage of high resolution VNIR data not provided by microwave remote sensing. The hyperspectral data has been applied successfully to map benthic vegetation by exploiting subtle spectral features due to phytopigment absorption in the VIS (e.g. Phinn et al., 2008; Kazemipour et al., 2012). Beyond the use of an oyster reef map for the management of wild oyster stocks as a resource for aquaculture, our classification method can be useful to simultaneously and accurately map benthic vegetation. In fact, the influence of oysters on benthic primary producers through top-down or bottom-up processes is an issue for shellfish ecosystems (Newell, 2004).

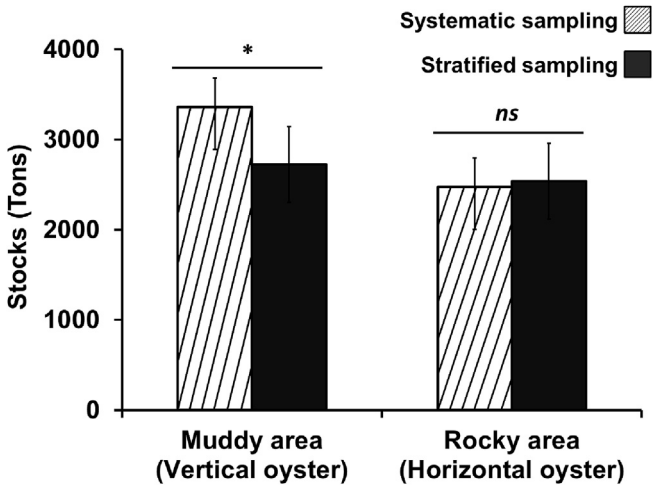

Fig. 8. Wild oyster stocks calculated for the large rocky area (site 2) colonized by horizontal oyster mapped Fig. 6 and rocky spots in the mudflat area (site 1) colonized by vertical oysters (Fig. 5 represents one of six similar rocky spots used for this stock estimation in muddy area). Two surface estimations have been used as explained Fig. 4, coupled to field biomass measurements. One is based on a stratified sampling applied to classes obtained by HySpex data and the other one is based on a systematic sampling applied to the total rocky areas delimited by SAR processing. The sampling effort was three times smaller for surfaces estimated with hyperspectral data ($n = 60$ vs. $n = 180$; see material & methods). Significant statistical analyses ($p < 0.05$) are indicated by *, while no significant difference are indicated by "*ns*" (*not-significant*).

4.2. Comparison between hyperspectral and multispectral data

The analysis of SAM classifications obtained from SPOT-5 satellite data showed that the reduced dimensionality of multispectral data combined with coarser pixels did not permit the identification of wild oyster reefs based on spectral shapes made up of three large VNIR spectral bands. Overall accuracies were below 50% for the two reef types. Schill et al. (2006) similarly reported that broadband sensors did not have the ability to map shellfish habitats. When HySpex data were convolved to simulate degraded spatial (10 m pixel with 160 spectral bands) or spectral (3 bands with 1 m pixel), the result showed that a high spectral resolution was greater than a high spatial resolution. This observation is shared by Underwood et al. (2007) who compared AVIRIS and Landsat sensors, or Girouard et al. (2004) for geological mapping. Many studies emphasized the finer discrimination obtained for various environments from narrow hyperspectral bands compared to a broadband resolution (e.g. wetlands vegetation Schmidt and Skimore, 2003; Zomer et al., 2009; benthic macroalgae Vahtmäe et al., 2006; coral reefs Kutser and Jupp, 2006; Botha et al., 2013). Nevertheless in this study, for rocky areas better results were observed for horizontal oysters detected using 1 m vs. 10 m pixels with the same 3 broad spectral bands. The increased spatial resolution probably reduced the number of mixed pixels that may be responsible for misclassifications. For tidal marshes vegetation, Belluco et al. (2006) indicated that spatial resolution affected classification accuracy greater than spectral resolution. In fact, a judicious choice of wavelengths can significantly improve the capability of a multispectral sensor (Hochberg and Atkinson, 2003; Hedley et al., 2004). Typically, three narrow bands in the visible range (496 nm, 586 nm and 675 nm) can be used to identify microphytobenthos (Combe et al., 2005). Although SPOT-5 data did not enable the identification of oyster reefs, the macroalgal belts were successfully classified (over 92%), and their spatial distribution was consistent with HySpex results. Guillaumont et al. (1993) have used SPOT imagery to map the distribution of the main intertidal macroalgae (*Ascophyllum nodosum*, *Fucus vesiculosus*; Phaeophyceae, Fucales), which are the species found in our study site. This means that reliable time-series of macroalgal distribution can be produced using multispectral data as has already been done for seagrass beds (Barillé et al., 2010). Temporal variations of the spatial distribution of macroalgae over the past 2 or 3 decades would be useful to investigate if these variations can be related to the invasion of intertidal areas by wild oysters in the early 1990's (Dutertre et al., 2010).

4.3. Spectral signatures of wild oysters

Field spectroradiometric measurements of the two types of oyster reefs - the first composed of vertical oysters growing on rocks in the muddy area; the second constituted by oysters growing horizontally on large rocky areas – revealed a surprising common spectral feature. All oyster shells showed an absorption band at 673 nm characteristic of the chlorophyll *a* absorption (Fig. 2), but there was no macroalgae colonizing the shells. This suggests the systematic presence of unicellular photoautotroph organisms that were not detectable visually. This explains why oyster shells colonized by a microalgal biofilm display spectral shapes in the visible wavelength range (400–700 nm) that resembles that of a microphytobenthos biofilm (Fig. 3). In vertical oyster reefs, there is a deposition of fine muddy particles on the shells and it is essentially this fine mud layer which is colonized by microalgae. The situation is different for the horizontal oyster reefs located on large rocky areas with a stronger hydrodynamism. There was less mud on the surface of the bright white shells which suggests that microalgae are closely associated to the shell itself. It is however beyond the scope of this work to elucidate this phenomenon, which is probably more complex than expected, since signs of endolithic microalgae were observed in some shells. In contrast to the similarities observed for visible wavelengths for the two types of reefs, horizontal oysters in rocky areas showed a higher reflectance at the NIR plateau (700–900 nm). The upwelling radiance is very likely stronger for the flat surfaces made up of horizontal shells. On the contrary, the three-tridimensional structure of the vertical reef creates shade and glint areas and a stronger bidirectional reflectance distribution function (BRDF) effect. This structure is likely characterized by multiple scattering. We tested *a posteriori* the effect of the sole geometric configuration (horizontal vs. vertical) with an experimental reconstitution with cleaned shells, and a higher NIR reflectance was indeed obtained with oysters organized horizontally. In fact, a higher VNIR albedo was observed, but the spectral shape was not modified. The presence of mud particles deposited on vertical oyster shells also contributed to their lower NIR spectral shape. Oyster signatures therefore share spectral similarities with microphytobenthos and mud which explains why confusion has arisen between these three classes. However, horizontal oysters had a stronger spectral identity and this higher NIR reflectance is never observed with mud and microphytobenthos (Méléder et al., 2003; Barillé et al., 2011).

4.4. Estimation of wild oyster stocks

Biomass estimation cannot be retrieved from remote sensing data only and field measurements are necessary (Kater and Baars, 2004). A previous stock assessment of wild oysters was performed in Bourgneuf Bay using photointerpretation and *in situ* biomass sampling (Cognie et al., 2006). Rocky areas were only analyzed generally, and neither oyster reefs nor macroalgal belts were identified. In this work, the discrimination of these surfaces with hyperspectral data was used to apply a stratified random sampling for the three main classes (Fig. 4). Compared to a

systematic sampling strategy, similar mean stocks and confidence intervals were obtained with a reduced sampling effort (Fig. 7). The stock was however underestimated for wild reefs in the muddy area due to the confusion previously described in spite of the high spectral resolution of HySpex. For this type of reefs composed of vertical oysters, it would be interesting to test radar data which detect surface roughness variations (e.g. Van der Wal et al., 2005; Gade et al., 2008). Dehouck et al. (2011) have shown the potential of TerraSAR-X in Arcachon Bay to map oyster-farming racks and oyster beds. Choe et al. (2012) used successfully multi-frequency polarimetric SAR data to map oyster reefs established on two mudflats in Korea from their particular texture. However, the distinction was made between oyster reef areas and bare sediment, and it would be interesting to see if their approach is effective for intertidal rocks characterized by a higher roughness. Gade et al. (2014) were also able to identify shellfish beds in the Wadden Sea with SAR data (oysters and mussels combined), but they could not reliably distinguish the two types of bivalve beds. From these works, it was suggested to combine radar with optical data to generalize oyster reef discrimination (Dehouck et al., 2011; Gade et al., 2014), but to our knowledge radar and hyperspectral data have not been associated yet. The limitation of hyperspectral data to identify oyster reefs in muddy areas must however be put into perspective. In Bourgneuf bay, this type of reef represents less than 2% (16 ha) compared to the rocky areas (1186 ha) where horizontal oysters can be observed. Along the French coast, wild oysters mostly colonized the lower part of rocky intertidal areas, often competing for space with mussel beds, and hyperspectral surveys should be adapted to map their spatial distribution.

5. Conclusion

Visible near-infrared remote sensing can be a useful tool for mapping wild oyster distribution in large intertidal areas for which it is difficult to obtain comprehensive ground data. However, as stated by Gade et al. (2014) for SAR imagery, our study showed that hyperspectral data could not solely be used to map the various types of oyster reefs. A combination of SAR/hyperspectral should be investigated. We must also remind the reader that there are subtidal oyster reefs (Kater and Baars, 2004) which are not detectable with these techniques in turbid coastal waters, and which would require the use of acoustic methods (Twichell et al., 2007). The intimate spectral mixtures observed at the level of oyster shells with the phytopigment absorption bands was a characteristic common to the two reef types (e.g. vertically and horizontally grown oysters). This characteristic seems to be associated with the amount of mud covering oyster reefs in varying degrees, conditioning the presence/absence of different types of microalgal biofilms: epipelic, epilithic or endolithic (Round et al., 1990). This variability should be investigated at a finer scale and we plan to use the HySpex camera in the laboratory to characterize these microscale spectral features. This knowledge may be useful for optimizing the spectral library of wild oysters and improving the mapping of their habitat.

Acknowledgments

The authors thank Ismaïl Benyoucef for his help during the field measurements in Bourgneuf Bay. We thank the CNES (Centre National d'Etudes Spatiales) for the provision of SPOT satellite images through the ISIS program and both OSUNA (Obervatoire des Sciences de l'Univers Nantes Atlantique) and the ACTIMAR company for the acquisition of the HySpex hyperspectral image. A part of this study was funded by the SMIDAP (Syndicat Mixte pour le Développement de l'Aquaculture et de la Pêche en Pays de la Loire). We thank Thomas Becker for correcting the English of this paper. This study was conducted as part of the PhD grant of Anthony Le Bris supported by the Ministère Français de la Recherche et de l'Enseignement Supérieur and awarded by the Fédération de Recherche IUML FR-CNRS of the University of Nantes in collaboration with the cluster of Excellence LabexMER.

References

Barillé, L., Mouget, J.-L., Méléder, V., Rosa, P., Jesus, B., 2011. Spectral response of benthic diatoms with different sediment backgrounds. Remote Sens. Environ. 115, 1034–1042. http://dx.doi.org/10.1016/j.rse.2010.12.008.

Barillé, L., Robin, M., Harin, N., Bargain, A., Launeau, P., 2010. Increase in seagrass distribution at Bourgneuf Bay (France) detected by spatial remote sensing. Aquat. Bot. 92, 185–194. http://dx.doi.org/10.1016/j.aquabot.2009.11.006.

Belluco, E., Camuffo, M., Ferrari, S., Modenese, L., Silvestri, S., Marani, A., Marani, M., 2006. Mapping salt-marsh vegetation by multispectral and hyperspectral remote sensing. Remote Sens. Environ. 105, 54–67. http://dx.doi.org/10.1016/j.rse.2006.06.006.

Benyoucef, I., Blandin, E., Lerouxel, A., Jesus, B., Rosa, P., Méléder, V., Launeau, P., Barillé, L., 2014. Microphytobenthos interannual variations in a north-European estuary (Loire estuary, France) detected by visible-infrared multispectral remote sensing. Estuar. Coast. Shelf Sci. 136, 43–52. http://dx.doi.org/10.1016/j.ecss.2013.11.007.

Botha, E.J., Brando, V.E., Anstee, J.M., Dekker, A.G., Sagar, S., 2013. Increased spectral resolution enhances coral detection under varying water conditions. Remote Sens. Environ. 131, 247–261. http://dx.doi.org/10.1016/j.rse.2012.12.021.

Brito, A.C., Benyoucef, I., Jesus, B., Brotas, V., Gernez, P., Mendes, C.R., Launeau, P., Dias, M.P., Barillé, L., 2013. Seasonality of microphytobenthos revealed by remote-sensing in a south European estuary. Cont. Shelf Res. 66, 83–91. http://dx.doi.org/10.1016/j.csr.2013.07.004.

Byrd, K.B., O'Connell, J.L., Di Tommaso, S., Kelly, M., 2014. Evaluation of sensor types and environmental controls on mapping biomass of coastal marsh emergent vegetation. Remote Sens. Environ. 149, 166–180. http://dx.doi.org/10.1016/j.rse.2014.04.003.

Chen, X., Vierling, L., 2006. Spectral mixture analyses of hyperspectral data acquired using a tethered balloon. Remote Sens. Environ. Spectr. Netw. 103, 338–350. http://dx.doi.org/10.1016/j.rse.2005.05.023.

Choe, B.-H., Kim, D., Hwang, J.-H., Oh, Y., Moon, W.M., 2012. Detection of oyster habitat in tidal flats using multi-frequency polarimetric SAR data. Estuar. Coast. Shelf Sci. 97, 28–37. http://dx.doi.org/10.1016/j.ecss.2011.11.007.

Cognie, B., Haure, J., Barillé, L., 2006. Spatial distribution in a temperate coastal ecosystem of the wild stock of the farmed oyster *Crassostrea gigas* (Thunberg). Aquaculture 259, 249–259. http://dx.doi.org/10.1016/j.aquaculture.2006.05.037.

Combe, J., Launeau, P., Carrere, V., Despan, D., Meleder, V., Barille, L., Sotin, C., 2005. Mapping microphytobenthos biomass by non-linear inversion of visible-infrared hyperspectral images. Remote Sens. Environ 98, 371–387. http://dx.doi.org/10.1016/j.rse.2005.07.010.

Congalton, R.G., 1991. A review of assessing the accuracy of classifications of remotely sensed data. Remote Sens. Environ. 37, 35–46. http://dx.doi.org/10.1016/0034-4257(91)90048-B.

Cotter, E., Malham, S.K., O'Keeffe, S., Lynch, S.A., Latchford, J.W., King, J.W., Beaumont, A.R., Culloty, S.C., 2010. Summer mortality of the Pacific oyster, *Crassostrea gigas*, in the Irish Sea: the influence of growth, biochemistry and gametogenesis. Aquaculture 303, 8–21. http://dx.doi.org/10.1016/j.aquaculture.2010.02.030.

Dehouck, A., Lafon, V., Baghdadi, N., Roubache, A., Rabaute, T., 2011. Potential of TerraSAR-X imagery for mapping intertidal coastal wetlands. In: Proceedings of the 4th TerraSAR-X Science Team Meeting. Oberpfaffenhofen.

Diederich, S., 2006. High survival and growth rates of introduced Pacific oysters may cause restrictions on habitat use by native mussels in the Wadden Sea. J. Exp. Mar. Biol. Ecol. 328, 211–227. http://dx.doi.org/10.1016/j.jembe.2005.07.012.

Diederich, S., 2005. Differential recruitment of introduced Pacific oysters and native mussels at the North sea coast: coexistence possible? J. Sea Res. 53, 269–281. http://dx.doi.org/10.1016/j.seares.2005.01.002.

Dutertre, M., Beninger, P.G., Barillé, L., Papin, M., Haure, J., 2010. Rising water temperatures, reproduction and recruitment of an invasive oyster, *Crassostrea gigas*, on the French Atlantic coast. Mar. Environ. Res. 69, 1–9. http://dx.doi.org/10.1016/j.marenvres.2009.07.002.

Elmore, A.J., Mustard, J.F., Manning, S.J., Lobell, D.B., 2000. Quantifying vegetation change in semiarid environments: precision and accuracy of spectral mixture analysis and the normalized difference vegetation index. Remote Sens. Environ. 73, 87–102.

FAO, 2006. The State of World Fisheries and Aquaculture 2006. Food and Agriculture Organization of the United Nations, Rome.

Forrest, B.M., Keeley, N.B., Hopkins, G.A., Webb, S.C., Clement, D.M., 2009. Bivalve aquaculture in estuaries: review and synthesis of oyster cultivation effects. Aquaculture 298, 1–15. http://dx.doi.org/10.1016/j.aquaculture.2009.09.032.

Gade, M., Alpers, W., Melsheimer, C., Tanck, G., 2008. Classification of sediments on exposed tidal flats in the German Bight using multi-frequency radar data.

Remote Sens. Environ 112, 1603–1613. http://dx.doi.org/10.1016/j.rse.2007.08.015. Remote Sensing Data Assimilation Special Issue.
Gade, M., Melchionna, S., Stelzer, K., Kohlus, J., 2014. Multi-frequency SAR data help improving the monitoring of intertidal flats on the German North sea coast. Estuar. Coast. Shelf Sci. 140, 32–42. http://dx.doi.org/10.1016/j.ecss.2014.01.007.
Girard, S., Pérez Agúndez, J.A., 2014. The effects of the oyster mortality crisis on the economics of the shellfish farming sector: preliminary review and prospects from a case study in Marennes-Oleron Bay (France). Mar. Policy 48, 142–151. http://dx.doi.org/10.1016/j.marpol.2014.03.024.
Girouard, G., Bannari, A., El Harti, A., Desrochers, A., 2004. Validated spectral angle mapper algorithm for geological mapping: comparative study between QuickBird and Landsat-TM. In: XXth ISPRS Congress, Geo-imagery Bridging Continents, Istanbul, Turkey, pp. 12–23.
Green, D.S., Rocha, C., Crowe, T.P., 2013. Effects of non-indigenous oysters on ecosystem processes vary with abundance and context. Ecosystems 16, 881–893. http://dx.doi.org/10.1007/s10021-013-9659-y.
Grizel, H., Héral, M., 1991. Introduction into France of the Japanese oyster (*Crassostrea gigas*). J. Cons. ICES J. Mar. Sci. 47, 399–403.
Grizzle, R.E., Adams, J.R., Walters, L.J., others, 2002. Historical changes in intertidal oyster (*Crassostrea virginica*) reefs in a Florida lagoon potentially related to boating activities. J. Shellfish Res. 21, 749–756.
Guillaumont, B., Callens, L., Dion, P., 1993. Spatial distribution and quantification of Fucus species and Ascophyllum nodosum beds in intertidal zones using spot imagery. In: Fourteenth International Seaweed Symposium. Springer, pp. 297–305.
Hedley, J.D., Mumby, P.J., Joyce, K.E., Phinn, S.R., 2004. Spectral unmixing of coral reef benthos under ideal conditions. Coral Reefs 23, 60–73. http://dx.doi.org/10.1007/s00338-003-0354-x.
Hochberg, E.J., Atkinson, M.J., 2003. Capabilities of remote sensors to classify coral, algae, and sand as pure and mixed spectra. Remote Sens. Environ. 85, 174–189. http://dx.doi.org/10.1016/S0034-4257(02)00202-X.
Kater, B.J., Baars, J.M.D., 2004. The potential of aerial photography for estimating surface areas of intertidal Pacific oyster beds (*Crassostrea gigas*). J. Shellfish Res. 23, 773–779.
Kazemipour, F., Launeau, P., Méléder, V., 2012. Microphytobenthos biomass mapping using the optical model of diatom biofilms: application to hyperspectral images of Bourgneuf Bay. Remote Sens. Environ. 127, 1–13. http://dx.doi.org/10.1016/j.rse.2012.08.016.
Krebs, C.J., 1989. Ecological Methodology. Harper and Row Publishers, New York.
Kruse, F.A., 2003. Preliminary results-hyperspectral mapping of coral reef systems using EO-1 Hyperion, Buck Island, US Virgin Islands. In: JPL Airborne Earth Science Workshop, pp. 157–173.
Kruse, F.A., Lefkoff, A.B., Boardman, J.W., Heidebrecht, K.B., Shapiro, A.T., Barloon, P.J., Goetz, A.F.H., 1993. The Spectral Image Processing System (SIPS) - Interactive Visualization and Analysis of Imaging Spectrometer Data.
Kutser, T., Jupp, D.L.B., 2006. On the possibility of mapping living corals to the species level based on their optical signatures. Estuar. Coast. Shelf Sci 69, 607–614. http://dx.doi.org/10.1016/j.ecss.2006.05.026. Salt Marsh Geomorphology: Physical and ecological effects on landform.
Leiper, I., Phinn, S., Roelfsema, C., Joyce, K., Dekker, A., 2014. Mapping coral reef benthos, substrates, and Bathymetry, using compact airborne spectrographic Imager (CASI) data. Remote Sens. 6, 6423–6445. http://dx.doi.org/10.3390/rs6076423.
Markert, A., Esser, W., Frank, D., Wehrmann, A., Exo, K.-M., 2013. Habitat change by the formation of alien Crassostrea-reefs in the Wadden sea and its role as feeding sites for waterbirds. Estuar. Coast. Shelf Sci. 131, 41–51. http://dx.doi.org/10.1016/j.ecss.2013.08.003.
Matthew, M.W., Adler-Golden, S.M., Berk, A., Richtsmeier, S.C., Levine, R.Y., Bernstein, L.S., Acharya, P.K., Anderson, G.P., Felde, G.W., Hoke, M.L., others, 2000. Status of atmospheric correction using a MODTRAN4-based algorithm. In: AeroSense 2000. International Society for Optics and Photonics, pp. 199–207.
Méléder, V., Barillé, L., Launeau, P., Carrère, V., Rincé, Y., 2003. Spectrometric constraint in analysis of benthic diatom biomass using monospecific cultures. Remote Sens. Environ. 88, 386–400. http://dx.doi.org/10.1016/j.rse.2003.08.009.
Mishra, D., Narumalani, S., Rundquist, D., Lawson, M., 2006. Benthic habitat mapping in tropical marine environments using QuickBird multispectral data. Photogramm. Eng. Remote Sens. 72, 1037–1048.
Mumby, P.J., Edwards, A.J., 2002. Mapping marine environments with IKONOS imagery: enhanced spatial resolution can deliver greater thematic accuracy. Remote Sens. Environ. 82, 248–257. http://dx.doi.org/10.1016/S0034-4257(02)00041-X.
Newell, R.I.E., 2004. Ecosystem influences of natural and cultivated populations of suspension-feeding bivalve molluscs: a review. J. Shellfish Res. 23, 51–61.
Nieuwhof, S., Herman, P.M.J., Dankers, N., Troost, K., van der Wal, D., 2015. Remote sensing of Epibenthic shellfish using synthetic aperture radar satellite imagery. Remote Sens. 7, 3710–3734. http://dx.doi.org/10.3390/rs70403710.
NOAA, 2003. Pilot Investigation of Remote Sensing for Intertidal Oyster Mapping in Coastal South Carolina (NOAA).
Pasqualini, V., Pergent-Martini, C., Pergent, G., Agreil, M., Skoufas, G., Sourbes, L., Tsirika, A., 2005. Use of SPOT 5 for mapping seagrasses: an application to Posidonia oceanica. Remote Sens. Environ. 94, 39–45. http://dx.doi.org/10.1016/j.rse.2004.09.010.
Pernet, F., Barret, J., Le Gall, P., Corporeau, C., Dégremont, L., Lagarde, F., Pépin, J., Keck, N., 2012. Mass mortalities of pacific oysters *Crassostrea gigas* reflect infectious diseases and vary with farming practices in the Mediterranean Thau lagoon, France. Aquac. Environ. Interact. 2, 215–237. http://dx.doi.org/10.3354/aei00041.
Phinn, S., Roelfsema, C., Dekker, A., Brando, V., Anstee, J., 2008. Mapping seagrass species, cover and biomass in shallow waters: an assessment of satellite multi-spectral and airborne hyper-spectral imaging systems in Moreton Bay (Australia). Remote Sens. Environ 112, 3413–3425. http://dx.doi.org/10.1016/j.rse.2007.09.017. Earth Observations for Marine and Coastal Biodiversity and Ecosystems Special Issue.
Purkis, S.J., Pasterkamp, R., 2004. Integrating *in situ* reef-top reflectance spectra with landsat TM imagery to aid shallow-tropical benthic habitat mapping. Coral Reefs 23, 5–20. http://dx.doi.org/10.1007/s00338-003-0351-0.
Quental, L.M., Sousa, A.J. de, Marsh, S., Abreu, M.M., 2013. Identification of Materials Related to Acid Mine Drainage Using Multi-source Spectra at S. Domingos Mine. SE Portugal.
Rosso, P.H., Ustin, S.L., Hastings, A., 2005. Mapping marshland vegetation of San Francisco Bay, California, using hyperspectral data. Int. J. Remote Sens. 26, 5169–5191.
Round, F.E., Crawford, R.M., Mann, D.G., 1990. The Diatoms: Biology and Morphology of the Genera. Cambridge University Press, Cambridge.
Schill, S.R., Porter, D.E., Coen, L.D., Bushek, D., Vincent, J., 2006. Development of an Automated Mapping Technique for Monitoring and Managing Shellfish Distributions. NOAAUNH Coop. Inst. Coast. Estuar. Environ. Technol. CICEET Durh. NH.
Schmidt, A., Wehrmann, A., Dittmann, S., 2008. Population dynamics of the invasive Pacific oyster *Crassostrea gigas* during the early stages of an outbreak in the Wadden sea (Germany). Helgol. Mar. Res. 62, 367–376. http://dx.doi.org/10.1007/s10152-008-0125-8.
Schmidt, K.S., Skidmore, A.K., 2003. Spectral discrimination of vegetation types in a coastal wetland. Remote Sens. Environ. 85, 92–108. http://dx.doi.org/10.1016/S0034-4257(02)00196-7.
Tompkins, S., Mustard, J.F., Pieters, C.M., Forsyth, D.W., 1997. Optimization of endmembers for spectral mixture analysis. Remote Sens. Environ. 59, 472–489. http://dx.doi.org/10.1016/S0034-4257(96)00122-8.
Troost, K., 2010. Causes and effects of a highly successful marine invasion: case-study of the introduced Pacific oyster *Crassostrea gigas* in continental NW European estuaries. J. Sea Res. 64, 145–165. http://dx.doi.org/10.1016/j.seares.2010.02.004.
Twichell, D.C., Andrews, B.D., Edmiston, H.L., Stevenson, W.R., 2007. Geophysical mapping of oyster habitats in a shallow estuary; Apalachicola Bay, Florida. U. S. Geol. Surv. Open-File Rep. 2006, 1381.
Underwood, E.C., Ustin, S.L., Ramirez, C.M., 2007. A comparison of spatial and spectral image resolution for mapping invasive Plants in coastal California. Environ. Manag. 39, 63–83. http://dx.doi.org/10.1007/s00267-005-0228-9.
Vahtmäe, E., Kutser, T., Martin, G., Kotta, J., 2006. Feasibility of hyperspectral remote sensing for mapping benthic macroalgal cover in turbid coastal waters—a Baltic sea case study. Remote Sens. Environ. 101, 342–351. http://dx.doi.org/10.1016/j.rse.2006.01.009.
Van der Wal, D., Herman, P.M.J., 2007. Regression-based synergy of optical, shortwave infrared and microwave remote sensing for monitoring the grain-size of intertidal sediments. Remote Sens. Environ. 111, 89–106. http://dx.doi.org/10.1016/j.rse.2007.03.019.
Van der Wal, D., Herman, P.M.J., Wielemaker-van den Dool, A., 2005. Characterisation of surface roughness and sediment texture of intertidal flats using ERS SAR imagery. Remote Sens. Environ. 98, 96–109. http://dx.doi.org/10.1016/j.rse.2005.06.004.
Yamano, H., Tamura, M., 2004. Detection limits of coral reef bleaching by satellite remote sensing: simulation and data analysis. Remote Sens. Environ. 90, 86–103. http://dx.doi.org/10.1016/j.rse.2003.12.005.
Zomer, R.J., Trabucco, A., Ustin, S.L., 2009. Building spectral libraries for wetlands land cover classification and hyperspectral remote sensing. J. Environ. Manag 90, 2170–2177. http://dx.doi.org/10.1016/j.jenvman.2007.06.028. The GlobWetland Symposium: Looking at wetlands from space The GlobWetland Symposium.